

# Experimental and Modeling Studies on the Filtration of SiO<sub>2</sub> Nanoparticles Aerosolized from Different Solvents

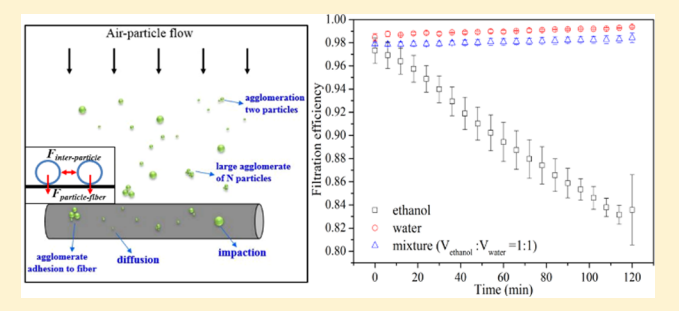
Youfeng Wang,<sup>†,§</sup>

Rongrong Cai,<sup>‡,§</sup> Lan Chen,<sup>\*,†</sup>

Xiaoyong Cai,<sup>†</sup> Rui Chen,<sup>†</sup> Chunying Chen,<sup>†</sup> and Guanglu Ge\*,†0

Supporting Information

ABSTRACT: The filtration performance of a fibrous filter in removing nano-SiO<sub>2</sub> aerosols atomized using different solvents including methanol, ethanol, 1-propanol, water, and the ethanol/water mixture has been investigated. Through discrete element method (DEM) simulation and filtration experiments, the efficiency variation caused by the combinative interaction of the particle-filter adhesion and interparticle attraction has been analyzed and verified. The adhesion force between the solvent-coated nanoparticles and the filter is considered as the key factor to influence their initial filtration efficiency and can be balanced by their interparticle interaction. The stronger the



adhesion, the higher the initial filtration efficiency. Primary aggregate is formed through the particle-fiber interaction, and further agglomerate is caused by particle migration on the fibers, i.e. secondary aggregate. Hydrogen bonding interaction is considered as the main factor causing interparticle secondary agglomeration, and plenty of OH groups existing in the nano-SiO2 aerosols yielded from alcohol promotes the particle secondary aggregation. As a result, the Brown diffusion capture of the filter is significantly abated, and the as-formed agglomerate is scraped off the filter surface by the alcohol molecules, causing the filtration efficiency decreases. This study highlights the surface affinity properties of nanoaerosols and their balance between particle-particle and particle-fiber interactions in the filtration process.

# ■ INTRODUCTION

Filtration is an effective approach to collect ultrafine particles, e.g. nanoparticles from air in the workplace and under atmospheric environment, which are difficult to remove from gaseous streams by other facilities. Consequently, fibrous filters have been widely used in facepiece respirators, indoor air conditioners, vehicular cabin air filters, and industrial gas cleaning devices for particle removal. It works by capturing the particles on the fiber when the aerosol passes through it.

Previous researchers have verified that the particle characteristics (e.g., size, size distribution, charge, shape, etc.), 1-3 the filter features (e.g., fiber diameter, packing density, fiber charge, etc.),4-6 and capture conditions (e.g., face velocity, relative humidity (RH), etc.)7-9 determine the specific capture mechanism (Brownian diffusion, interception, inertial impaction, and/or electrostatic forces) and the morphology of the particle deposition thereby influencing the performance of the filter. 10-14 For Brownian diffusion, dendrite-like particle aggregates with open pore structures are the majority due to the even distribution and agglomeration of the particles around the fiber. Compact dendrite structures are formed facing the flow due to inertial impaction, while more open structures accompanying striking dendrites are often related to the interception capture mechanism. In the case of electret fibers, chain-like agglomerates are formed by uncharged particles, and higher dendrites concentrated in a more limited area on the fiber surface are generated by charged particles. 15 The deposits formed on the fibers also become part of the filter structure and hence affect the filtration efficiency.

The particle collection process is basically determined by the complex interactions between particle-external field, particlefiber, and particle-particle. The electrostatic force and hydrodynamic drag force from external electrostatic and airflow fields mainly contribute to the particle transportation. The adhesion forces of particle-fiber and particle-particle are the short-range forces that would have significant effects on the particle collision, aggregation, capture, and consequently the filtration performance. Many experimental phenomena might be contributed to the difference in adhesion; for example, the effect of RH on the filtration of nanoparticles is still a controversial question, and a number of relevant topics have

Received: April 15, 2018 Revised: July 11, 2018 Accepted: July 12, 2018 Published: July 12, 2018



<sup>&</sup>lt;sup>†</sup>CAS Key Laboratory of Standardization and Measurement for Nanotechnology, CAS Center for Excellence in Nanoscience, National Center for Nanoscience and Technology, Beijing 100190, P. R. China

<sup>\*</sup>Key Laboratory of Enhanced Heat Transfer and Energy Conservation of Education Ministry, School of Chemistry and Chemical Engineering, South China University of Technology, Guangzhou 510640, P. R. China

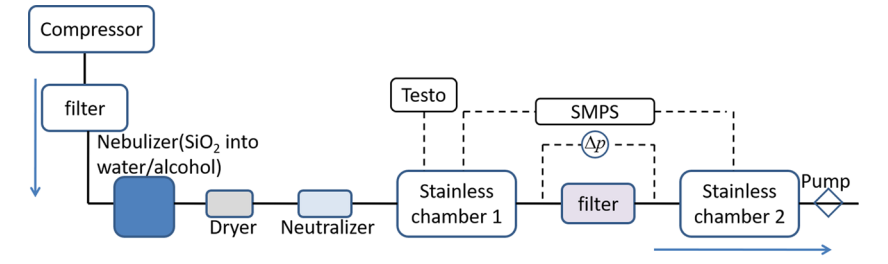


Figure 1. Scheme of experimental filtration test system.

been reviewed and summarized in Table S1. When the capillary force between the nanoparticles and the filter surface is considered, the efficiency increases with RH due to the enhancement of the adhesion between nanoparticles and the surface, 16 while the efficiency of the filter with preloaded particles decreases with RH increase owing to the shrinking of agglomerates if the interparticle interaction is considered.<sup>17</sup> The variations of filtration efficiencies changing with RH have not been mentioned by previous works<sup>2,18</sup> due to the low moisture regained for glass fiber and the insufficient particles deposited on the filters to cause a detectable difference in filtration efficiency. Meanwhile, the recent modeling proved that the larger adhesion force (i.e., larger Hamaker constant) would lead to looser particle dendrites, faster deposition rates, and better filtration efficiency. 13 The previous research only focuses on the particle-fiber adhesion and does not consider the combinative effect from the interparticle and particle-fiber interactions on the filtration. There is still a marked gap between the theory and experiment on the relationship between the particle collection efficiency and the adhesion parameters.

It is quite common to examine the filtration performance by generating aerosols through nebulization. Water and some organic solvents are most widely used in nebulization. Many researchers have conducted the solvent effect on the filtration, and most of them focus on electret filters. 19-21 The efficiency decrease of the filter has been observed after it is treated by organic solvents and high affinity between filter and the solvents benefits for charge neutralization. As known, the particle size distribution and surface adhesion can be affected by the physicochemical properties of the solvent, which further influence the particle transportation, aggregation, and deposition, as well as the filtration performance. The solvent difference may also have an effect on the nanoaerosols during their generation and filtration by commercial available filters. However, less attention has been paid to it. It is, therefore, necessary to quantitatively assess the filtration performance for the particles nebulized from these solvents prior to its application in industrial scale.

In this study, we aim to clarify the efficiency deterioration problem for the filters in relation to the adsorption and desorption of the nanoparticles atomized from nonaqueous solvents, e.g. alcohol on them. Filtration evaluation is performed using nano-SiO $_2$  aerosol atomized by different solvents respectively, such as methanol, ethanol, 1-propanol, water, and the ethanol/water mixture. To better understand the filtration mechanism and investigate the filtration behavior, the lattice Boltzmann modeling coupled with the discrete element method (LB-DEM) is adopted to simulate the deposition of the nanoparticles aerosolized from ethanol and

water on the fiber surface. The modeling results confirm that the particle adhesion plays a key role in the filtration behavior.

## **■ EXPERIMENTAL SECTION**

Testing System and Protocol. All the filtration performance measurements were conducted in a testing system as shown in Figure 1. It consists of an air compressor, air purification filters, a nebulizer, a diffusion dryer, a neutralizer, and a filter penetration measurement system. The testing process involves the generation of nanoaerosol, the aerosol passing through the testing chambers, and the measurement of the particle concentrations and size distributions before (chamber 1) and after (chamber 2) the filter. The volume of the two identical cylindrical chambers is  $\sim 1.6$  L. The temperature and RH inside the stainless chamber 1 were recorded by a multifunction measuring instrument (Testo, model 435) within an accuracy of  $\pm 0.3$  °C for temperature and  $\pm 2\%$  for RH. The temperature ranges from 5 to 31 °C, and the RH was adjusted from 19% to 50% in the experiments.

The polydisperse aerosols were generated via a six-jet collision atomizer (TSI model 9306) under an inlet pressure of 10 psi (3.7 L/min), followed by passage through a diffusion dryer and an electrical charge neutralizer (TSI model 3087) to reach a Boltzmann charge distribution. The nano-SiO<sub>2</sub> particles were synthesized in acetone by a patented technology developed by us<sup>22</sup> using tetraethyl orthosilicate (TEOS) as the silica source and tetramethylammonium hydroxide (TMAH) as the catalyst. The SiO<sub>2</sub> nanoparticles were suspended by dispersing a given amount of SiO<sub>2</sub> powder into ultrapure water, methanol, ethanol, 1-propanol, and the ethanol/water mixture (1:1 v/v) respectively using an ultrasonic probe. In order to achieve thorough drying and remove the most solvent molecules, different desiccants in the diffusion dryer were loaded for the different solvents, e.g. using 3A molecular sieves for the water, 5A molecular sieves for the alcohol, and the mixture of 3A and 5A molecular sieves for the ethanol/water removal, respectively. The as-generated aerosols were analyzed on a copper grid by transmission electron microscopy (TEM, T20, TECNAI Inc., USA) and on the filter by scanning electron microscopy (SEM, Zeiss, Merlin).

The aerosol flow at the rate of 3.0 L/min and the face velocity at 4.65 cm/s were controlled by a pump with critical orifice. The pressure drop was measured during the experiment using a digital manometer (TSI 5825). The number concentration and size distributions of the aerosol were recorded and analyzed using a Scanning Mobility Particle Sizer (SMPS, TSI model 3936), consisting of a water-based Condensation Particle Counter (CPC, TSI model 3788, USA), an Electrostatic Classifier (EC, TSI model 3080, USA), and a Differential Mobility Analyzer (DMA, TSI model 3081, USA). The size detection limit of SMPS is 10 to 414 nm, and its

upper limit for concentration is  $1.0 \times 10^7$  particles/cm.<sup>3</sup> Zero calibration with high efficiency particulate air filter (HEPA) was conducted prior to use. The measurements were alternately made in both upstream and downstream chambers before/after the filter unit during the process and then used to determine filter efficiency at the time interval during loading. Considering the particle loss caused by diffusion in the transportation process, the filtration efficiency presented here was corrected by the particle concentration in the chamber without filter. The measurements were repeated three times for each experiment.

The commercially available flat filter of 37 mm-diameter made of polypropylene fiber is classified as H13 (99.97% MPPS Efficiency for particles >0.3  $\mu$ m). The fiber diameter and thickness of the filters were determined according to their SEM images, and the measured mean value is about 1.52 and 491  $\mu$ m, respectively. The fiber packing density is 2.85%. In order to neutralize the charge and remove impurities on the filters if any, the media was submerged in isopropyl alcohol for 2 h and dried naturally in a fume hood for 48 h, by which the charge on the filter is considered to be completely neutralized referring to the previous reports. <sup>21,23</sup> Physical deformation of the filter is negligible as seen by SEM in this work.

**Characterization and Analysis.** Thermal gravimetric analysis (TGA) was conducted to determine the solvent amount covered on the aerosols and/or filter surfaces to calculate the derived adhesion forces. The analyzed samples include the pristine powder, the aerosol particles collected after nebulization from ethanol and water, and after desiccation, filters after exposure to ethanol and water vapor. The experiments are performed using a TG-DTA7300 with an accuracy of  $\pm 1~\mu g$ . The balance and sample compartments are purged with nitrogen. Surface area analysis of the particles was performed using a micromeritics BET analyzer (ASAP 2020HD88) at 77 K by nitrogen sorption.

## MODELING

To specifically model the aerosol dynamics of the transportation, agglomeration, and deposition process through the air filter, the lattice Boltzmann coupled discrete element method (LB-DEM) is employed.

**The Air Flow.** Solutions of the airflow are calculated using the lattice Boltzmann method. The domain discretization model D3Q15<sup>24</sup> and the single relaxation Bhatnagar-Gross-Krook (BGK) scheme<sup>25</sup> are employed. Accordingly, the particle distribution functions ( $f_i$ ) in dimensionless units of density), as functions of nondimensional space (**X**) and time (t), are expressed as

$$f_i(\mathbf{X} + \mathbf{e}_i \delta t, t + \delta t) = f_i(\mathbf{X}, t) - \frac{\delta t}{\tau} [f_i(\mathbf{X}, t) - f_i^{\text{eq}}(\rho, \mathbf{u})]$$
 (1)

where  $\mathbf{e}_i$  is discrete direction vectors, as illustrated in Figure S1.  $\tau$  is the dimensionless relaxation time, which is used to give a favorable relationship between the kinetic air viscosity  $(\nu)$  and time step between iterations  $(\delta t)$ , respectively. For a given node spacing of  $\delta x$ , the relation is

$$\nu = (\tau - 0.5) \frac{\delta x^2}{3\delta t} \tag{2}$$

 $f_i^{\rm eq}(\rho, {\bf u})$  is the equilibrium density distribution function, which is given by

$$f_i^{\text{eq}}(\rho, \mathbf{u}) = \mathbf{w}_i \rho \left( 1 + 3 \frac{\mathbf{e}_i - \mathbf{u}}{C^2} + 9 \frac{(\mathbf{e}_i - \mathbf{u})^2}{2C^4} - \frac{3u^2}{2C^2} \right)$$
(3)

where  $\mathbf{w}_i$  is a direction-orientated weight coefficient, e.g.  $w_0 = 2/9$ ;  $w_{1-6} = 1/9$ ;  $w_{7,-14} = 1/72$  according to different directions.<sup>24</sup> The density  $\rho$  and the velocity  $\mathbf{u}$  at space (X) can be calculated by

$$\rho = \sum_{i=0}^{14} f_i(\mathbf{X})$$

$$\mathbf{u} = \frac{\sum_{i=0}^{14} f_i(\mathbf{X}) \mathbf{e}_i}{\rho(\mathbf{X})}$$
(4)

**The Particle Flow.** During the filtration process, a nanoparticle is mainly subjected to a hydrodynamic drag force  $(\mathbf{F}_D)$ , a Brownian diffusion force  $(\mathbf{F}_B)$ , a possible electrostatic force  $(\mathbf{F}_E)$ , and an adhesive force  $(\mathbf{F}_A)$  acting on the particle by surrounding colliding particles. The particle trajectory is considered by resolving the equation of translation according to Newton's second law

$$m_{\rm p} \frac{\mathrm{d}\mathbf{u}_{\rm p}}{\mathrm{d}t} = \mathbf{F}_{\rm D} + \mathbf{F}_{\rm B} + \mathbf{F}_{\rm E} + \mathbf{F}_{\rm A} \tag{5}$$

where  $\mathbf{u}_{\mathrm{P}}$  is the particle velocity. Here the rotation of nanoparticle is omitted.

The hydrodynamic drag force is dominated by viscous drag. According to Stokes' law, the drag force on a spherical particle can be expressed<sup>26</sup>

$$\mathbf{F}_{\mathrm{D}} = \frac{3\pi d_{\mathrm{p}}\mu}{C_{c}} (\mathbf{u} - \mathbf{u}_{\mathrm{p}}) \tag{6}$$

where  $C_c = 1 + Kn(1.275 + 0.4e^{-1.1/Kn})$  is an empirical Cunningham slip correction factor.  $^{27}$   $Kn = 2\lambda/d_{\rm f}$  is the fiberbased Knudsen number.  $\lambda$  is the mean free path of gas molecules and is about 65 nm.  $\mu$  is the air dynamic viscosity.  $d_{\rm f}$  and  $d_{\rm p}$  are the fiber diameter and particle diameter, respectively.

The Brownian force is a vital one in nanoparticle filtration. Wang et al.<sup>28</sup> have discussed the combined effects of hydrodynamic drag and Brownian motion on aerodynamic performance for nanoparticles. The results show that the theory-based expression for Brownian motion is reliable, provided that the "slip" of gas molecules on the particle surface is properly included. Here, the random Brownian force is calculated as a white noise process<sup>29</sup>

$$\mathbf{F}_{\mathrm{B}} = \theta \sqrt{\frac{216\rho\nu k_{\mathrm{B}}T}{\pi\rho_{\mathrm{p}}^{5}d_{\mathrm{p}}^{5}\Delta t C_{c}}} \tag{7}$$

where  $\theta$  is a zero-mean, unit-variance independent Gaussian random number.  $\rho_{\rm p}$  is the particle density.  $\Delta t$  is the particle time step.

Since the filter is considered to be neutralized in the model, the electrostatic force can be omitted. The adhesive forces are short-range forces, which become significant only if the particle distance is small enough. The following major adhesive forces are thought to affect the particle—particle and particle—fiber interactions, such as (i) van der Waals force, (ii) capillary force due to surface tension of the formed liquid bridges, and (iii) chemical bonds, etc., where both the interparticle and

particle—fiber interactions are considered. To simplify the description, the cylindrical fiber is also referred to as "particle" in the following.

(1). van der Waals Force  $F_{vdW}$ . The van der Waals force  $F_{vdW}$  between two spherical particles with diameters of  $d_{p1}$  and  $d_{p2}$  can be calculated by<sup>30</sup>

$$F_{\text{vdW}} = \frac{H}{12D^2} \frac{d_{\text{pl}} d_{\text{p2}}}{d_{\text{pl}} + d_{\text{p2}}}$$
(8)

where H is the Hamaker constant between the two particles, and D is the minimum separation distance between two particles. In this study, the aerosol particle is covered with a solvent layer. The van der Waals force between two particles 1 and 2 with solvent layers 3 and 4 across medium 5 (see Figure S2) is given by<sup>31</sup>

$$F_{\text{vdW}} = \frac{d_{\text{pl}} d_{\text{p2}}}{12(d_{\text{p1}} + d_{\text{p2}})} \left[ \frac{H_{435}}{D^2} - \frac{\sqrt{H_{242} H_{535}}}{(D + \delta 1)^2} - \frac{\sqrt{H_{131} H_{545}}}{(D + \delta 2)^2} + \frac{\sqrt{H_{131} H_{242}}}{(D + \delta 1 + \delta 2)^2} \right]$$
(9)

where  $\delta 1$  and  $\delta 2$  are the thickness of the solvent layers around particles 1 and 2. The typical values of the Hamaker constants for polypropylene, SiO<sub>2</sub>, ethanol, and water in the air are  $6.5 \times 10^{-20}$  J,  $6.3 \times 10^{-20}$  J,  $4.2 \times 10^{-20}$  J, and  $3.7 \times 10^{-20}$  J, respectively.<sup>32</sup>

(2). Capillary Force  $F_c$ . Liquid bridges can be formed and become significant when the particle is surrounded by a layer of solvent. Pakarinen et al.<sup>33</sup> have pointed out that the capillary force for nanoparticles depends on the relative humidity, and the surface tension force also depends on the nanoparticle size, which influences the total capillary force for small nanoparticles. To quantify the effect of relative humidity, a correction factor  $\beta$ , which is defined as the ratio of the capillary force calculated for 100% relative humidity to the actual capillary for a certain relative humidity level, is introduced. Thus, the capillary force  $F_c$  for hydrophilic materials as a function of the surface tension of liquid is 16

$$F_{\rm c} = 2\beta\pi\sigma d_{\rm p} \tag{10}$$

where  $\sigma$  is the surface tension of the solvent (0.0735 N/m for water, 0.0218 N/m for ethanol).  $\beta$  can be determined using the experimental data by Pakarinen et al.<sup>33</sup> The capillary force for other sizes and relative humidity can be calculated by extrapolation. The detail values of  $\beta$  in different cases are shown in Table S2.

(3). Hydrogen Bond Force  $F_{H\ bond}$ . The short-range adhesion force from hydrogen bonding between hydroxyl groups on the SiO<sub>2</sub> particle surface  $F_{H\ bond}$  is considered. A key characteristic of the SiO<sub>2</sub> surface is that it is covered with silanol (SiOH) groups at room temperature. When using alcohol and water as solvents, the hydroxylated particle surfaces can act as hydrogen bond acceptors.<sup>34</sup> The adhesion forces due to hydrogen bonding as a function of particle diameters for the SiO<sub>2</sub> particles are displayed in Figure S3, where the  $F_{H\ bond}$  (SiO<sub>2</sub> in alcohol) is calculated according to the ratio of 5:7 for the O–H–O and the H–O–R hydrogen bonds.<sup>35</sup>

**The Simulation Setup.** A Matlab program has been developed to generate the virtual fibrous structure, which is an approximate representative for a real filter. It is assumed that

fiber arrangement is three-dimensionally random, and all fibers have the in-plane fiber orientation in random angle and the same diameter in all cases. A virtual 3-D model of the fibrous filter with fiber packing density of 2.85% is shown in Figure 2.

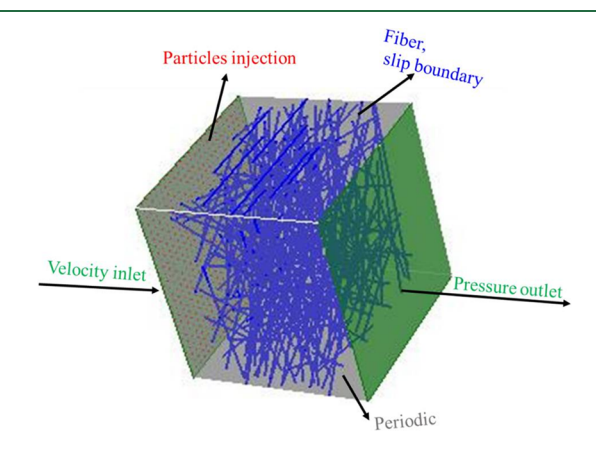


Figure 2. Scheme of the computational domain and boundary conditions.

During the numerical simulation, the velocity-inlet and pressure-outlet boundaries are used for the inlet and outlet of the airflow, respectively. These boundary conditions in LBM are handled by the nonequilibrium extrapolation method.<sup>36</sup> The uniform airflow inlet boundary condition has been set at a distance of  $6d_{\rm fb}$  upstream of the filter, while the outlet boundary condition has been set at a distance of  $6d_{\rm fb}$ downstream of the filter, to avoid the interruption from the region where strong velocity and pressure gradients are expected. Meanwhile, the boundaries of other sides of the computational domain are set to be the periodic boundary conditions based on the structural characteristics of the fibrous filter. These boundary conditions are also displayed in Figure 2. For the airflow on the fiber surfaces, a slip boundary condition is applied. In LB implementation, the slip-reflection model<sup>37</sup> is adopted.

The particles are injected from the inlet boundary at a constant rate for a given volume concentration. In the study, the particle volume concentration is set to be 0.0001. The periodic boundary conditions for particle flow are applied for the other four sides of the domain. If the particles move beyond the computational region, they are not considered in the numerical model.

#### ■ RESULTS AND DISCUSSION

**Experimental Results.** Characterization of Aerosols Atomized from Different Solvents. SMPS measurement and extensive electron microscopy studies are performed on the asproduced SiO<sub>2</sub> aerosols out of different solvents. The morphology of the collected aerosols on the copper grid is shown in Figure S4. It can be seen from TEM images that the water-based atomization can conglobate SiO<sub>2</sub> particles, while the ethanol-based one simply aggregates these particles on the copper grid. The results indicated that the interparticle interaction is different for the particles from water with that from ethanol. TGA analyses show that the thickness of the ethanol and water molecules covering the particles is ~10 and 4.9 nm, respectively as shown in Table S3. The initial normalized size distribution of the atomized nanoparticles out of different solvents in stainless chamber 1 is shown in Figure

3. The error bars are obtained from three batches of repeated experiments and used to qualitatively demonstrate the

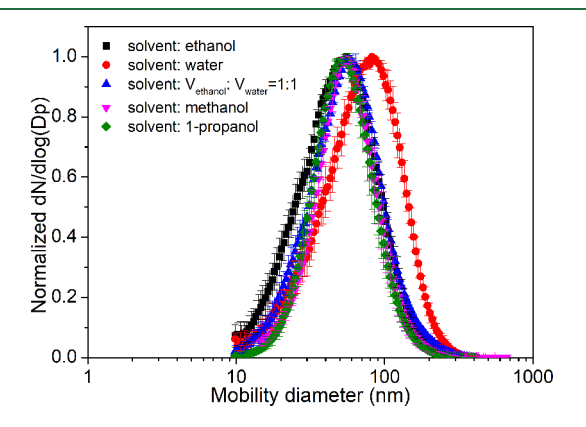


Figure 3. Normalized size distributions of nano-SiO<sub>2</sub> aerosol particles atomized from different solvents (methanol, ethanol, 1-propanol, water, and the ethanol/water mixture (1:1 in v/v)). Error bars represent the repeated batches of experiments.

temporal stability and reproducibility. The mode diameter (peak) of the SiO<sub>2</sub> aerosols atomized from different solvents are 55, 55, 53, 57, and 82 nm, respectively for methanol, ethanol, 1-propanol, the ethanol/water mixture, and water with a geometric standard deviation of 1.62, 1.81, 1.60, 1.75, and 1.85 respectively. The temperature-corrected surface tensions for methanol, ethanol, 1-propanol, the ethanol/water mixture (1:1 in volume), and water are 24.33, 21.82, 23.84, 29.25, and 72.01 mN/m, respectively under the experimental conditions.<sup>38</sup> The smaller the surface tension, the smaller the formed droplet size, and the easier the formed liquid film is to be disintegrated in the atomization process, thus causing the peak diameter of the aerosol particles atomized from alcohol and the ethanol/water mixture much smaller than that from water. Table S4 summarizes some experimental results reported in the literature on the aerosol particles generated by spray-drying of different solvents. It concludes that the particle size and morphology are influenced by the evaporation rate and surface tension of the solvent, the solubility of the solutes in the solvent, and the interaction between the solute and solvent, as well as the concentration of the solute for certain circum-

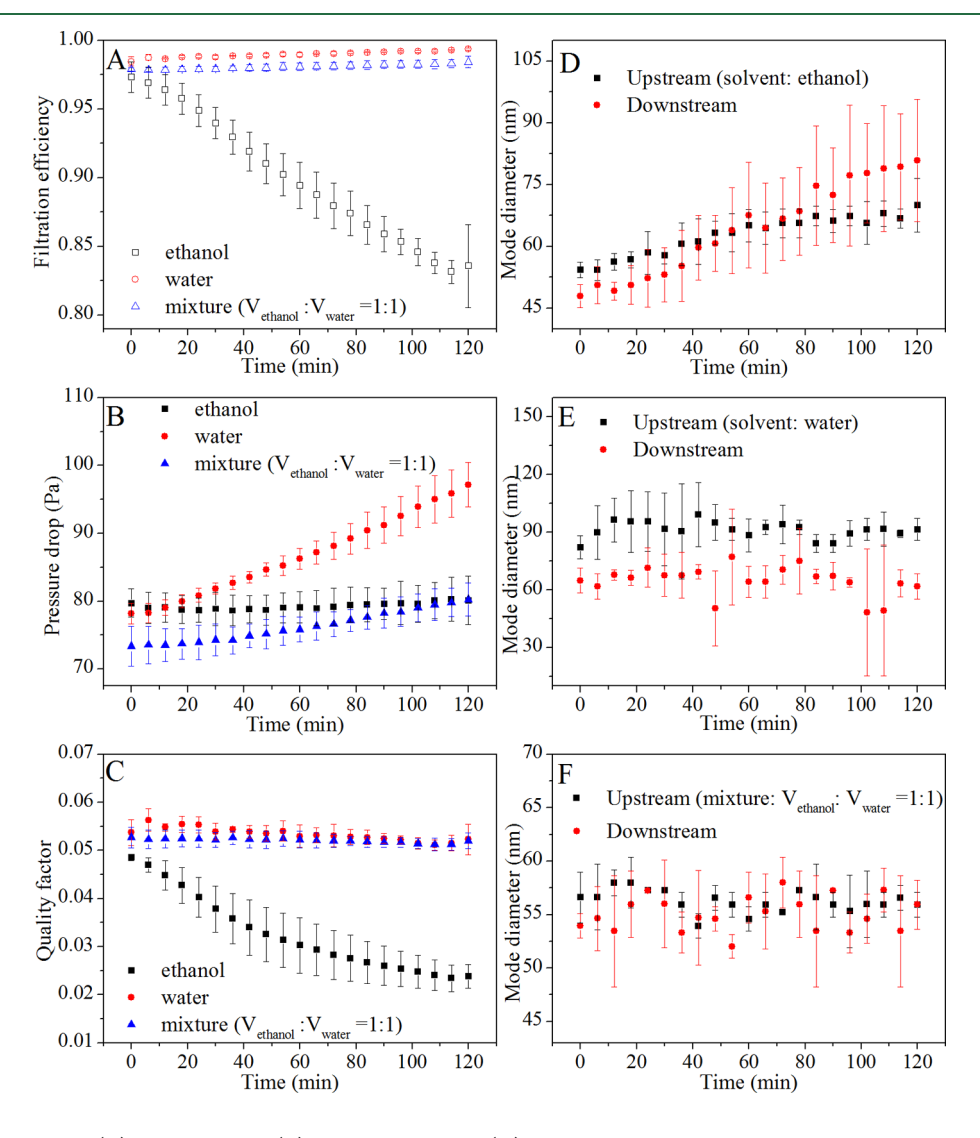


Figure 4. Filtration efficiency (A), pressure drop (B), and quality factor (C) of the filtration tests for aerosol particles from different solvents; the change of mode diameter of the aerosol particles atomized from ethanol (D), water (E), and the ethanol/water mixture (F) in upstream and downstream around the filters.

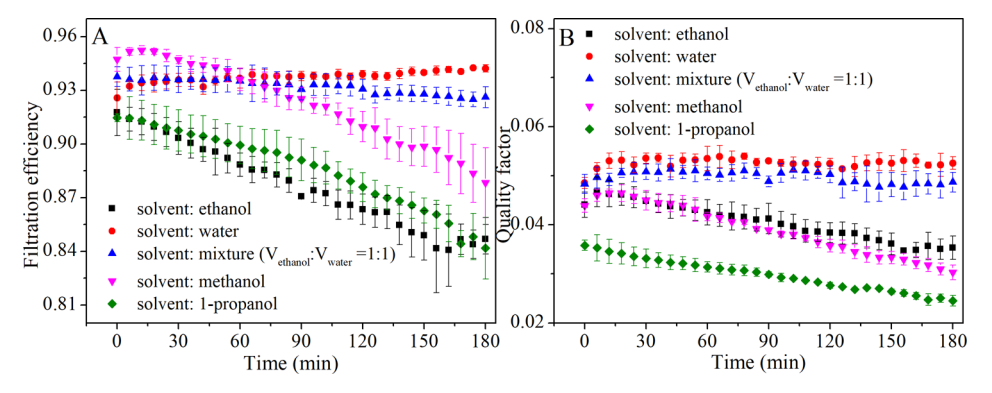


Figure 5. Filtration efficiency and quality factor of the aerosol particles collected by the charge-neutralized filters.

stances. For this work, the different solvents used also make the composition and morphology of the surface layer on the particles different, which may lead to different filtration performance.

Filtration Tests of SiO<sub>2</sub> Aerosols from Different Solvents. Filtration tests are continued for 2 h for all the original fibrous filters. Figures 4(A-C) present the filtration efficiency, the pressure drop, and the quality factor of the nano-SiO<sub>2</sub> aerosols atomized from different solvents, respectively. It is observed that the filtration efficiency and pressure drop increase with time for the aerosol atomized from water and the ethanol/ water mixture, which is due to the reason that the as-deposited particles could act as new nucleation sites for the succeeding particle aggregation. Whereas, the filtration efficiency significantly decreases with the time, and the pressure drop almost remains constant for the aerosols atomized from ethanol. It has been reported that the efficiency increases by mechanical capture, while it decreases by electrostatic capture with the increase of the filter loading.<sup>39</sup> To further verify whether the effect of electrostatic capture is the dominant factor, filtration tests are continued for 3 h with charge-neutralized filters to conduct the experiments. In addition, the effect of methanol and 1-propanol as the solvent on filtration has also been investigated in order to examine whether different hydrophobic/hydrophilic moiety ratios can significantly influence its filtration behavior. First, the initial filtration efficiency in Figure 5A is about 4% lower than that obtained in Figure 4A, and the efficiency decreases with time are almost the same as the particles produced from ethanol. It is implied that the charge loss by ethanol wetting is not the dominant reason for the decrease of its filtration efficiency. A similar phenomenon has also been observed by Xiao et al.<sup>21</sup> where alcoholic aerosol causes a small decrease in the collection efficiency for the meltblown polypropylene electrets filter fabrics. Thus, the electrostatic capture effect will not be discussed in the following section. Second, the change tendency, i.e. the slope for the filtration efficiency and quality factor of the particles atomized from three alcohols, is quite similar as seen in Figure 5. Previous reports claimed that methanol, ethanol, and 1propanol can form an ~15 nm layer on silica surface with the hydrogen-bonded macrocluster structure. 40,41 This suggests that the liquid-liquid molecular attraction between the alcohol-coated aerosol particles might be similar for the different alcohols as observed by the similar slopes of the efficiency decay curves, while the adhesion between the particles and the filter is different for different solvents. According to the Young-Dupré equation, 42 the adhesion between the filter and the particles atomized from different

solvents can be estimated by the combined function of the surface tension and contact angle. The stronger the adhesion is, the higher the initial filtration efficiency, i.e. intercept is for the particles atomized from different solvents (Figure 5). According to the temperature-corrected surface tension and measured contact angle,<sup>43</sup> the strongest adhesion to the PP filter is obtained for the aerosol atomized from methanol, while it decreases in the order of methanol, the ethanol/water mixture, water, 1-propanol, and ethanol, which is basically in agreement with that of the initial filtration efficiency (intercept) change. It appears that the adhesion property rather than the length of the hydrocarbon hydrophobic chain of these alcohols has a significant effect on the filtration behavior.

Particle size distributions as a function of mobility diameter of the SiO<sub>2</sub> aerosols upstream and downstream (before/after) the test filter are shown in Figure S5. The shift from 48 to 74 nm of the peaks is seen for SiO<sub>2</sub> aerosols atomized from ethanol after 2 h. Figures 4(D-F) show the change of mode diameter (MD) for the SiO2 aerosols atomized from ethanol, water, and the ethanol/water mixture, respectively. The MD almost remains unchanged with time for the aerosol particles from water and the ethanol/water mixture. The average MD for the aerosol particles from the ethanol/water mixture ranges from 52 to 58 nm (Figure 4F), while the average MD is 82 to 100 nm in the upstream and 48 to 77 nm in the downstream for the aerosol particles from water within 2 h of the testing time, which is an indicator that the filters are more effective for the larger particle size (>80 nm) at the selected face velocity. Unexpectedly, the MD for the aerosol particles from ethanol increases with the time in both the upstream and downstream, and the growth rate in the downstream is faster. The average MD grows from 54 to 70 nm in the upstream and 47 to 81 nm in the downstream, which suggests that particle agglomeration occurs during the transportation of the aerosol particles and intensifies after impacting with the particles collected on the fibers. In a batched drying process, the adsorption capacity of the molecular sieves decreases gradually with the filtration time, and the remaining alcohol vapor concentration, therefore, increases. The hydrogen-bonding interaction makes the particles more adhesive with the increase of the alcohol vapor concentration, and then, their average mode diameter grows from 54 to 68 nm after 84 min of filtration time as shown in Figure 4D. However, no significant increase in their average mode diameter has been observed from 84 to 120 min since the attraction reaches its maximum capability when the alcohol vapor concentration exceeds its critical concentration under the experimental conditions. 41 Hence, particle adhesion

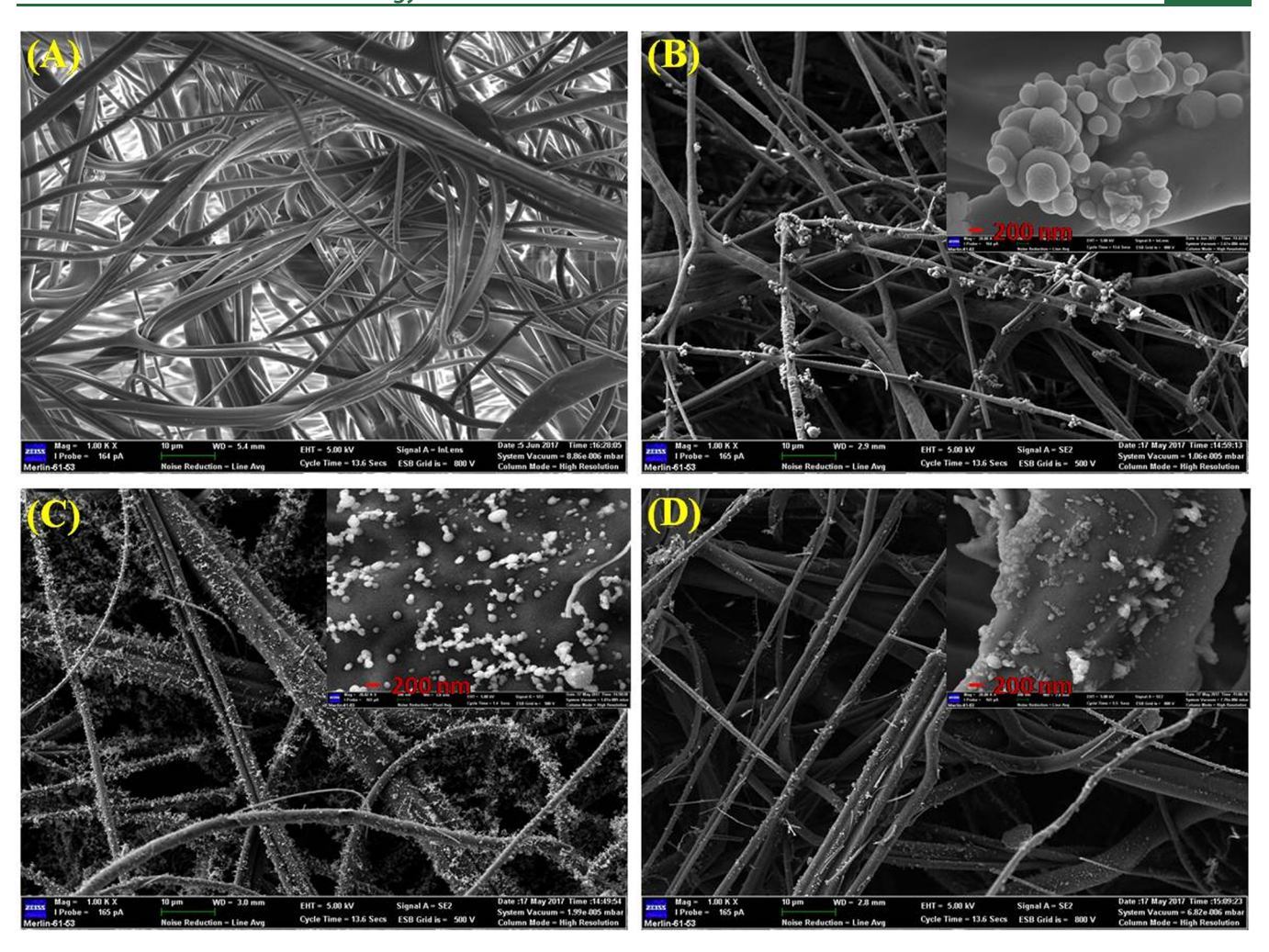


Figure 6. SEM images of filters: blank filter (A) and filters exposed to particles atomized from ethanol (B), water (C), and the ethanol/water mixture (1:1 inv/v) (D) after 2 h of filtration.

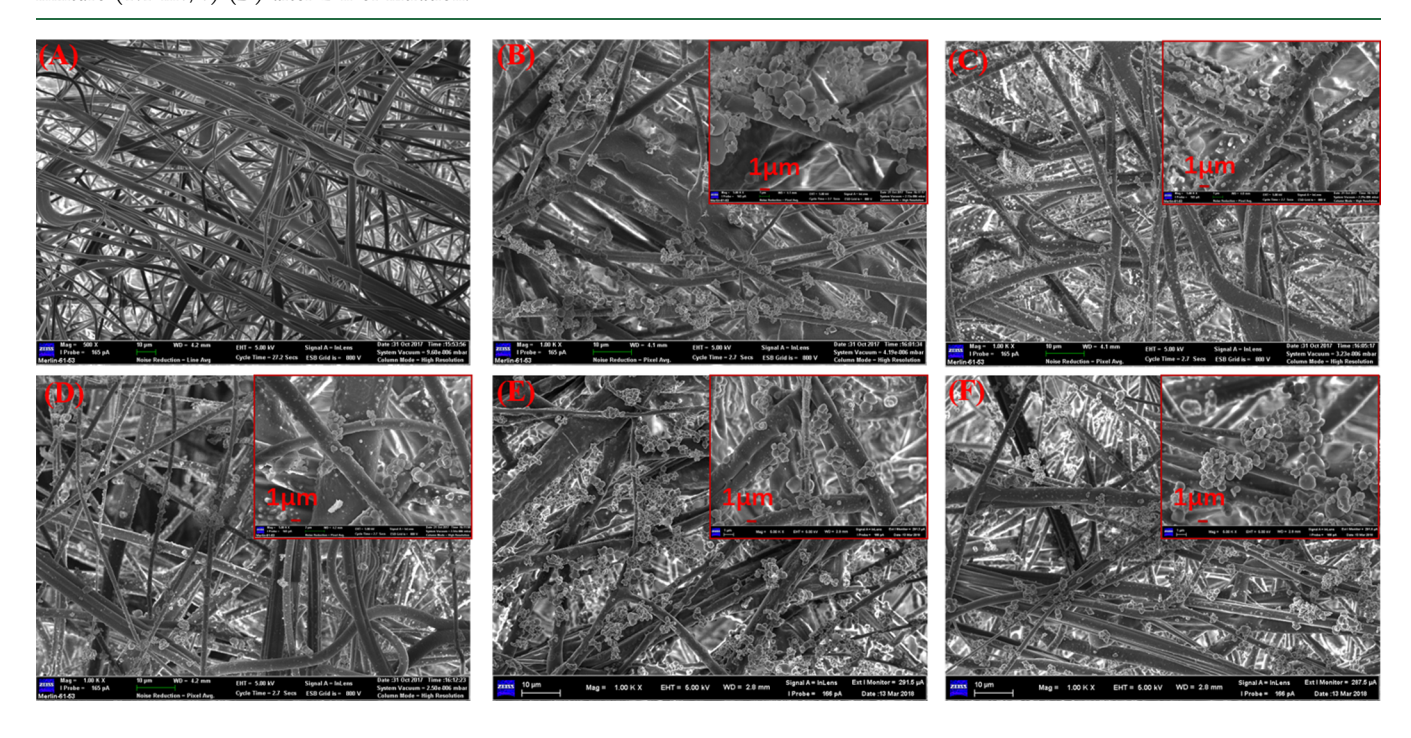


Figure 7. SEM images of the charge-neutralized filters: blank filter (A) and filters exposed to particles atomized from ethanol (B), water (C), the ethanol/water mixture (1:1 v/v) (D), methanol (E), and 1-propanol (F) after 3 h of filtration.

emerges as the dominant reason for the filtration performance change on the aerosol particles produced from ethanol.

Recently many researchers have paid attention to the influence of agglomerate morphology on the collection efficiency as summarized in Table S5. It is widely accepted that the agglomerates with larger interception length are more conducive to be intercepted and captured compared to the spherical particles. Buha et al. 44 found that for the diffusiondominant small particles (<70 nm), the morphology of the particles does not play a significant role on the filtration efficiency change. The morphology of the collected particles on the original and charge-neutralized filters used in this study is depicted in Figures 6 and 7, respectively. Distinctly, the aerosols atomized from alcohol tend to aggregate severely on the filter while those atomized from water and the ethanol/ water mixture tend to distribute evenly on the fibers. The aggregate structures from water look more dendritic than those from the ethanol/water mixture due to the larger particle size.11 Diffusion and interception are, therefore, considered as the dominant mechanisms for the filtration tests. Unlike the previous studies, the filtration efficiency for agglomerates derived from alcohol is lower than those derived from water and the ethanol/water mixture. It is supposed that the larger adhesion forces among the particles atomized from alcohol result in the formation of larger agglomerates. When the agglomerates become large to a certain extent on the fiber surface, the fluid drag force might be strong enough to make the bulk agglomerates scraped off the fiber. To further investigate the effect of alcoholic aerosol on the filters loaded with particles, additional experiments are performed by passing the aerosols atomized from water in the first 2 h and then passing the ethanol aerosol for another 2 h through the same filter. The morphology formed before and after the ethanol aerosol exposure appears in Figure S6. It is observed that the particles collected on the filter lose their spherical shape and coalesce when the filter is loaded with particles exposed to the ethanol aerosol, which is similar to that impact of RH on the filters loaded with nanoparticles, 7,18 where the adherent force originating from surface tension of the dissolved nanoparticles caused coalescence of the nanoparticles when RH increases. The coalescence of the loaded particles after ethanol aerosol exposure is probably due to the chemical bonds formed with ethanol molecules have higher interaction energy. As proposed by Gallyamov et al., 45 a competitive adsorption onto the filter membrane exists between the SiO<sub>2</sub> nanoparticles and alcohol molecules, where the more amphiphilic alcohol wins the competition and scrapes the loaded particles off the surface of the filter when the alcohol molecules are adsorbed in the sites where the particles locate due to stronger affinity to the filter. However, the SiO<sub>2</sub> nanoparticles tend to form compact agglomerates on the filter in order to minimize the adhesion interaction energy between the particles and the particleoccupied surface under these conditions. The interparticle interaction might domain in the filtration for the aerosol particles produced from ethanol. The efficiency deterioration in filtration of the nano-SiO2 aerosol after being nebulized from ethanol is further clarified in the following section.

**Simulation Results.** To disclose the inherent mechanism for the difference in the capture and agglomeration of nano-SiO<sub>2</sub> aerosols atomized from different solvents, a 3-D filtration model considering interparticle and particle—fiber interactions specifically is employed. The parameter and their value used in the simulation are provided in Table 1. The aerosol particle

sizes are discretized into 10 bins in the simulation, and their distribution (fraction) is determined by the experiments, as seen in Figure 8.

Table 1. Parameters and Their Values in the Simulation

parameter	value		
surface tension, $\sigma/(N/m)$	0.0735 (water), 0.0218 (ethanol)		
filter thickness, $t/(\mu m)$	30		
fiber packing density, $\alpha$	0.0285		
fiber diameter, $d_{ m fb}/(\mu{ m m})$	1.52		
air density, $\rho/(kg/m^3)$	1.293		
air kinetic viscosity, $\nu/(m^2/s)$	$14.8 \times 10^{-6}$		
particle density, $\rho_p/(kg/m^3)$	2200		
particle volume concentration, c	≈0.0001		
Boltzmann constant, $k_{\rm B}/({\rm m^2~kg~s^{-2}~K^{-1}})$	$1.38 \times 10^{-23}$		
face velocity, $U_0/(m/s)$	0.0465		
temperature, $T/(K)$	300		
relative humidity, $RH/(\%)$	30%		

To save computational time, the filter thickness is set to 30  $\mu$ m. Figure 9 shows the variation of the filtration efficiency, pressure drop, and quality factor of the PP filter with the time. Nano-SiO<sub>2</sub> aerosols atomized from ethanol and water are compared. As seen, the variation tendency for the nano-SiO<sub>2</sub> aerosols from the two solvents is well fitted with the experimental results (Figure 4). The filtration efficiency of nano-SiO<sub>2</sub> aerosols (from water) increases gradually with time, since the as-captured particles would act as active sites for the incoming SiO<sub>2</sub> aerosol deposition. The growth of dendrite size and the increase in the solid content inside the PP filter lead to a fast increase in pressure drop and a significant decrease in the quality factor with the time for the aerosol produced from water. However, the performance is quite different for the nano-SiO2 aerosols atomized from ethanol. The filtration efficiency of the SiO<sub>2</sub> aerosols (from ethanol) decreases sharply with time, and the pressure drop remains unchanged, resulting in a significant decrease in quality factor. As known, the filtration performance of the filter largely depends on the aerosol dynamics through the filter.

As illustrated in Figure 10, the aerosol particles are first driven by the hydrodynamic force and Brownian force to the fibrous filter, and the collisions among them form the particle agglomerates by the adhesion forces. If the particle—fiber interaction is stronger than the interparticle one, only the primary aggregate is generated on the fibers through the diffusion and impaction of the aerosol particles/agglomerates. The secondary agglomerate may be formed via the particles/agglomerates migration on the fibers driven by the interparticle if it is strong enough to pull the particles off the fiber. Consequently, the aerosol particle dynamic behavior is considered to be regulated by both the macroscopic forces and the short-range adhesive forces.

The strengths of both the macroscopic forces and of interparticle adhesive forces that affect the aerosol particle transportation and deposition are calculated in the simulation. As summarized in Table 2, the relative orders of magnitude of these forces and their changes with the diameter of the nano-SiO<sub>2</sub> aerosols are compared. It confirms that the Brownian force is much stronger than the drag force for nano-SiO<sub>2</sub> aerosols transportation, and it increases sharply with decreasing particle size. Distance-sensitive van der Waals force is a relatively small adhesion force, since the nano-SiO<sub>2</sub>

**Environmental Science & Technology** 

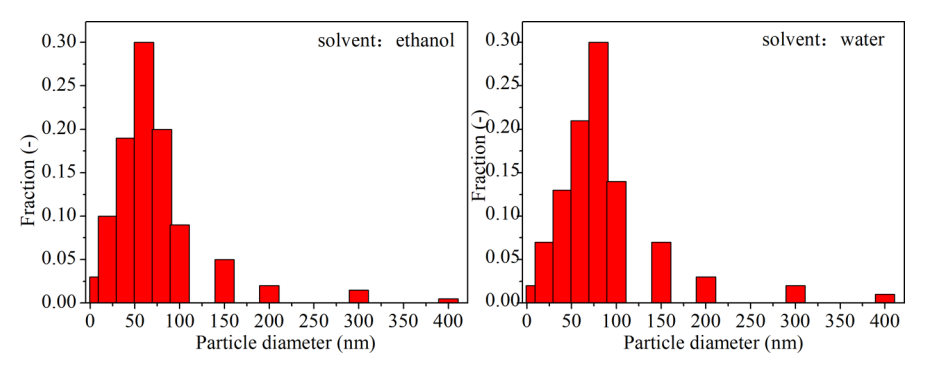
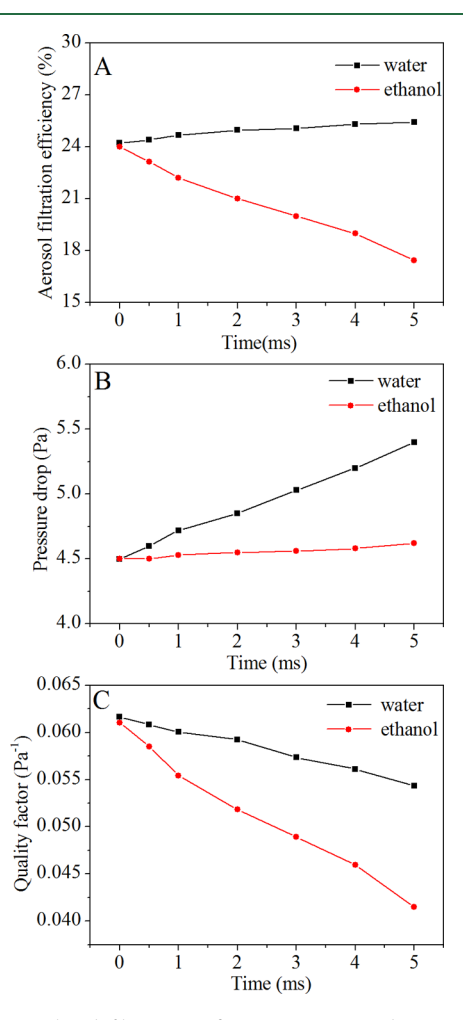


Figure 8. Discrete aerosol particle sizes and their distributions in the simulation.



**Figure 9.** Simulated filtration efficiency, pressure drop, and quality factor varying with time for the SiO<sub>2</sub> aerosol particles from different solvents.

aerosols are covered and separated by solvent molecules. According to the experimental results, the solvent coverage thicknesses are  $\sim\!10$  and 4.9 nm respectively for ethanol and water. The capillary force plays an important role in particle—fiber interaction. As compared to Table 2, the capillary interaction between the PP fiber and the nano-SiO $_2$  aerosol from water is stronger than that from ethanol due to its larger surface energy, thus the filtration efficiency for the nano-SiO $_2$  aerosols produced from ethanol is smaller. The hydrogen bond might be formed between the nano-SiO $_2$  aerosols under moisture conditions and has a significant effect on aerosol

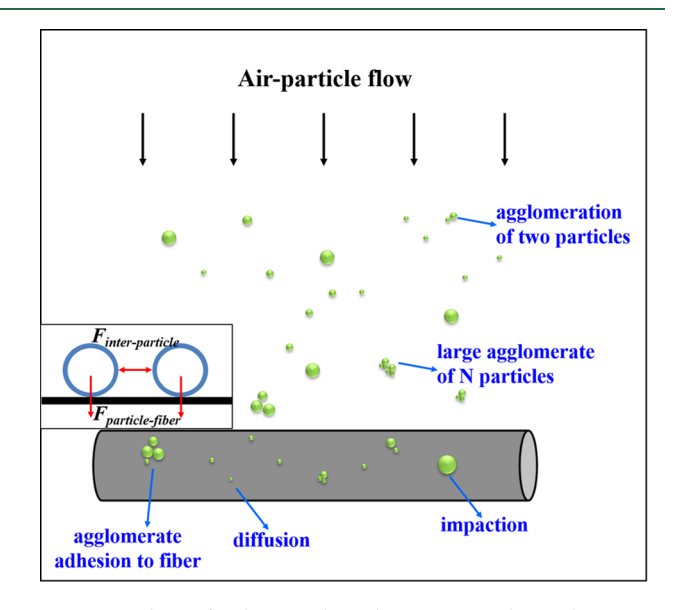


Figure 10. Scheme for the particle agglomeration and particle capture.

aggregation. The strength of the hydrogen bonds  $F_{Hbond}$  for the  $SiO_2$  from ethanol is larger than that from water. Consequently, it can be inferred that the particle agglomeration is more severe for the  $SiO_2$  from ethanol. This explains why the size significantly increases for the nano- $SiO_2$  aerosols produced from ethanol during the filtration.

The morphology of aerosol particle deposition on fibrous filters for the nano-SiO<sub>2</sub> aerosols from water and ethanol is modeled and compared in Figure 11. As seen, the nano-SiO<sub>2</sub> aerosols from water are distributed evenly on the fiber surface, which indicates that Brown diffusion dominates the particle capture. For the nano-SiO<sub>2</sub> from ethanol, particle agglomeration becomes evident. The model prediction is consistent with that observed in the experiments. The aerosol agglomeration can influence the nano-SiO<sub>2</sub> collection in two aspects: (1) the Brown diffusion capture is weakened due to the increase of the agglomerate size; (2) some large agglomerates are more easily scrapped off the fiber surface by the hydrodynamic drag force. Therefore, the nano-SiO<sub>2</sub> agglomerates from ethanol become significant, and their filtration efficiency decreases with time.

This study has systematically investigated the influence of different solvents (water, methanol, ethanol, 1-propanol, and the ethanol/water mixture) on the nebulized nano-SiO $_2$  aerosol filtered through fibrous filters. The difference in filtration behavior can be understood in terms of the difference of the interaction at the solid/liquid interface with the surfaces

Table 2. Force Type and Strength Acting on One Single Particle with a Diameter  $d_{\rm p}$ 

			Fvdw/(N)			FHbond/(N)
$d_{\rm p}/({\rm nm})$	$F_{\mathrm{D}}/(\mathrm{N})$	$F_{\rm B}/({ m N})$	particle-fiber	particle-particle	$F_{\rm c}/({ m N})$	particle-particle
10	$1.44 \times 10^{-14}$	≈10 <sup>-9</sup>	$5.30 \times 10^{-13}$ (ethanol)	$6.56 \times 10^{-14} \text{ (ethanol)}$	$1.05 \times 10^{-9}$ (ethanol)	$5.28 \times 10^{-8}$ (ethanol)
			$2.21 \times 10^{-12}$ (water)	$2.73 \times 10^{-13}$ (water)	$3.56 \times 10^{-9}$ (water)	$3.77 \times 10^{-8} \text{ (water)}$
50	$1.44 \times 10^{-14}$	$\approx 10^{-10}$	$2.58 \times 10^{-12}$ (ethanol)	$3.28 \times 10^{-13}$ (ethanol)	$5.27 \times 10^{-9}$ (ethanol)	$4.07 \times 10^{-7} \text{ (ethanol)}$
			$1.08 \times 10^{-11} \text{ (water)}$	$1.37 \times 10^{-12} \text{ (water)}$	$1.78 \times 10^{-8} \text{ (water)}$	$2.91 \times 10^{-7} \text{ (water)}$
100	$4.35 \times 10^{-14}$	$\approx 10^{-11}$	$5.0 \times 10^{-12}$ (ethanol)	$6.56 \times 10^{-13} \text{ (ethanol)}$	$1.05 \times 10^{-8}$ (ethanol)	$9.8 \times 10^{-7}$ (ethanol)
			$2.08 \times 10^{-11} \text{ (water)}$	$2.73 \times 10^{-12}$ (water)	$3.56 \times 10^{-8}$ (water)	$7.0 \times 10^{-7} \text{ (water)}$
200	$1.13 \times 10^{-13}$	$\approx 10^{-12}$	$9.43 \times 10^{-12} \text{ (ethanol)}$	$1.31 \times 10^{-12}$ (ethanol)	$2.11 \times 10^{-8}$ (ethanol)	$2.35 \times 10^{-6}$ (ethanol)
			$3.93 \times 10^{-11}$ (water)	$5.47 \times 10^{-12} \text{ (water)}$	$7.11 \times 10^{-8}$ (water)	$1.68 \times 10^{-6} \text{ (water)}$
400	$2.63 \times 10^{-13}$	$\approx 10^{-13}$	$1.69 \times 10^{-11} \text{ (ethanol)}$	$2.63 \times 10^{-12} \text{ (ethanol)}$	$4.22 \times 10^{-8}$ (ethanol)	$5.61 \times 10^{-6}$ (ethanol)
			$7.03 \times 10^{-11} \text{ (water)}$	$1.09 \times 10^{-11} \text{ (water)}$	$1.42 \times 10^{-7} \text{ (water)}$	$4.01 \times 10^{-6} \text{ (water)}$

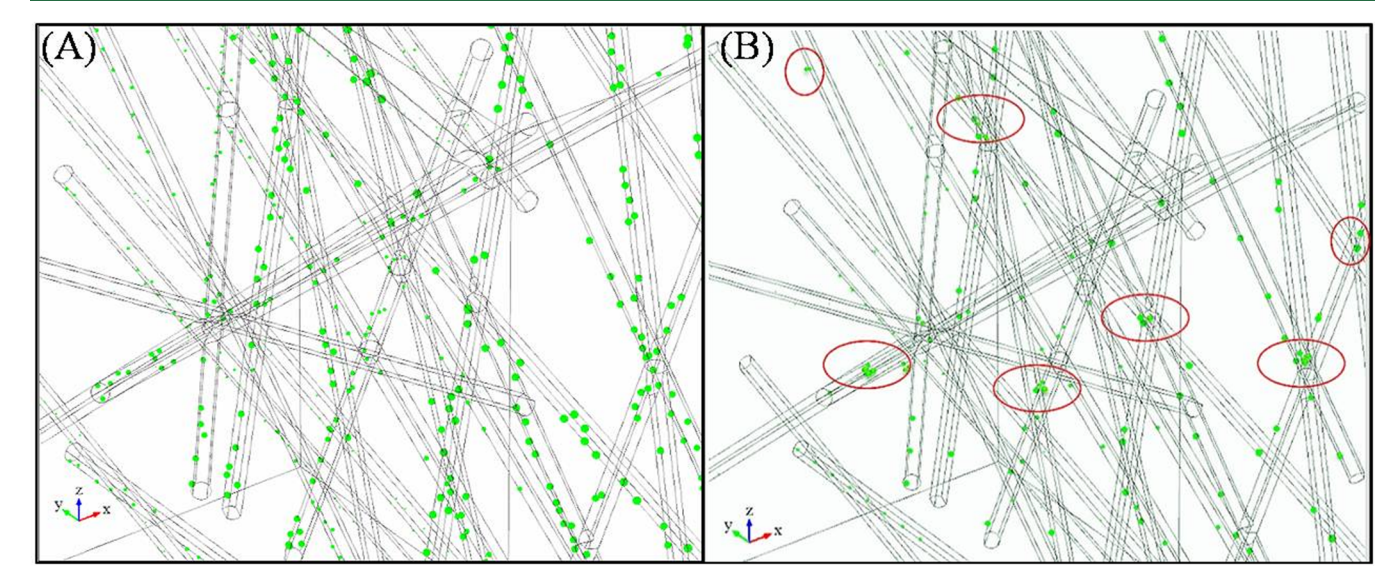


Figure 11. Simulated morphology of the particle deposited on fibrous filter for the SiO<sub>2</sub> aerosols from water (A) and ethanol (B).

covered by different solvent molecules. Both the experimental and simulated results in this work provide an insight into the complementary effect of both the interparticle attraction and particle—fiber adhesion on the filtration processes, which would be useful to explain some disputes, such as the impact of RH on the aerosol nanoparticle filtration.

## ENVIRONMENTAL IMPLICATIONS

There are thousands of companies globally involved in the production and application of nanomaterials, which unavoidably causes some environmental and health concerns. For example, the chemical storage room has been found to be a significant source of incidental nanoaerosol production within the workplace, generating a rate of 63.8 particles/cm<sup>3</sup>/s with a number of VOCs. 46 How to insulate these ultrafine materials from workers and clean them efficiently in a more facile manner is a challenge for both industry and academia. Solventassisted dust capture technologies, e.g. the wet electrostatic scrubbers, 47 are considered as a convenient and economic way to purify the indoor air in workplace. Among them, solventassisted filtration (i.e., wet filtration) is one of the most widely used approaches. However, the solvation effect of the ultrafine particles on their filtration mechanism is not very clear until now. Therefore, an appropriate model needs to be built to better describe the filtration mechanism in terms of particle size, surface status, and composition. The research not only

deepens the understanding on the solvent-involved filtration mechanism but also provides guidance on how to choose the filter (hydrophobic/hydrophilic) needed for the air cleaning in industry or any indoor environment with high levels of volatile organic compounds (VOCs) and nanoparticles. Among them, silica is the most massive engineered nanoparticles, which involves the use of various solvents during the production, processing, and applications. In fact, many indoor air pollutants typically consist of gases or ultrafine particles of different physical and chemical properties that can harm people's health; therefore, it is urgently needed to develop a more comprehensive and customized filtration technology to more effectively collect these engineered particles.

To the best of our knowledge, it is the first time to elucidate that the presence of alcohol can reduce rather than increase the nanoparticle filtration efficiency not like water does. Both the experimental and modeling results show that the particle-filter adhesion and interparticle attraction synergistically play a role in the filtration, whose mechanism has not been well-illustrated previously, where this work will generate new knowledge on this topic.

#### ASSOCIATED CONTENT

## S Supporting Information

The Supporting Information is available free of charge on the ACS Publications website at DOI: 10.1021/acs.est.8b02010.

Particle morphology of the SiO<sub>2</sub> aerosol particles collected on the substrates, TGA results of the particles, as well as the calculation of the hydrogen-bonding force and the schematic for van der Waals between particles, summaries of literature on the spray-drying generation of particles, and influence of RH and aggregate morphology on the filtration performance (PDF)

#### AUTHOR INFORMATION

#### **Corresponding Authors**

\*E-mail: chenlan@nanoctr.cn. \*E-mail: gegl@nanoctr.cn.

#### **ORCID** ®

Youfeng Wang: 0000-0003-4088-1714 Lan Chen: 0000-0002-7243-5244 Chunying Chen: 0000-0002-6027-0315 Guanglu Ge: 0000-0002-2460-6686

#### **Author Contributions**

§Y.W. and R.C. contributed equally.

#### **Notes**

The authors declare no competing financial interest.

# ACKNOWLEDGMENTS

This work was funded by the National Natural Science Foundation of China (Grant No. 21707025, Grant No. 51506058), the project "Industrial Nano-manufacturing Focus" by Chinese Academy of Sciences (XDA09040400), and the Science Foundation of Guangdong Province in China (2015A030310358).

# REFERENCES

- (1) Cheng, Y. S.; Zhou, Y. Effects of size and shape on filtration of TiO<sub>2</sub> nanoparticles. Aerosol Sci. Technol. 2017, 51 (8), 972-980.
- (2) Kim, C. S.; Bao, L.; Okuyama, K.; Shimada, M.; Niinuma, H. Filtration efficiency of a fibrous filter for nanoparticles. J. Nanopart. Res. 2006, 8 (2), 215-221.
- (3) Tang, M.; Thompson, D.; Chang, D.-Q.; Chen, S.-C.; Pui, D. Y. H. Filtration efficiency and loading characteristics of PM<sub>2.5</sub> through commercial electret filter media. Sep. Purif. Technol. 2018, 195, 101-
- (4) Yamada, S.; Seto, T.; Otani, Y. Influence of filter inhomogeneity on air filtration of nanoparticles. Aerosol Air Qual. Res. 2011, 11 (2),
- (5) Raynor, P.; Kim, B.; Ramachandran, G.; Strommen, M.; Horns, J.; Streifel, A. Collection of biological and non-biological particles by new and used filters made from glass and electrostatically charged synthetic fibers. Indoor air 2008, 18 (1), 51-62.
- (6) Bortolassi, A. C. C.; Guerra, V. G.; Aguiar, M. L. Characterization and evaluate the efficiency of different filter media in removing nanoparticles. Sep. Purif. Technol. 2017, 175, 79-86.
- (7) Montgomery, J. F.; Green, S. I.; Rogak, S. N. Impact of relative humidity on HVAC filters loaded with hygroscopic and nonhygroscopic particles. Aerosol Sci. Technol. 2015, 49 (5), 322-331.
- (8) Xu, B.; Wu, Y.; Lin, Z.; Chen, Z. Investigation of air humidity affecting filtration efficiency and pressure drop of vehicle cabin air filters. Aerosol Air Qual. Res. 2014, 14 (3), 1066-1073.
- (9) Shi, B.; Ekberg, L. Ionizer assisted air filtration for collection of submicron and ultrafine particles—evaluation of long-term performance and influencing factors. Environ. Sci. Technol. 2015, 49 (11), 6891-6898.
- (10) Kanaoka, C.; Emi, H.; Hiragi, S.; Myojo, J. Morphology of particulate agglomerates on a cylindrical fiber and a cllection efficiency of a dust loaded fiber, 2nd Int, Aerosol Conf., Berlin, 1986.

- (11) Kasper, G.; Schollmeier, S.; Meyer, J. Structure and density of deposits formed on filter fibers by inertial particle deposition and bounce. J. Aerosol Sci. 2010, 41 (12), 1167-1182.
- (12) Dunnett, S. J.; Clement, C. F. Numerical investigation into the loading behaviour of filters operating in the diffusional and interception deposition regimes. J. Aerosol Sci. 2012, 53, 85-99.
- (13) Cai, R.-R.; Zhang, L.-Z. Modeling of dynamic deposition and filtration processes of airborne particles by a single fiber with a coupled lattice Boltzmann and discrete element method. Build. Environ. 2016, 106, 274-285.
- (14) Ji, J.; Bae, G.; Kang, S.; Hwang, J. Effect of particle loading on the collection performance of an electret cabin air filter for submicron aerosols. J. Aerosol Sci. 2003, 34 (11), 1493-1504.
- (15) Kanaoka, C.; Hiragi, S.; Tanthapanichakoon, W. Stochastic simulation of the agglomerative deposition process of aerosol particles on an electret fiber. Powder Technol. 2001, 118 (1), 97-106.
- (16) Givehchi, R.; Tan, Z. The effect of capillary force on airborne nanoparticle filtration. J. Aerosol Sci. 2015, 83, 12-24.
- (17) Montgomery, J. F.; Rogak, S. N.; Green, S. I.; You, Y.; Bertram, A. K. Structural change of aerosol particle aggregates with exposure to elevated relative humidity. Environ. Sci. Technol. 2015, 49 (20), 12054-12061.
- (18) Hwang, G. B.; Lee, J. E.; Nho, C. W.; Lee, B. U.; Lee, S. J.; Jung, J. H.; Bae, G.-N. Short-term effect of humid airflow on antimicrobial air filters using Sophora flavescens nanoparticles. Sci. Total Environ. 2012, 421-422, 273-279.
- (19) Kim, J.; Hinestroza, J. P.; Jasper, W.; Barker, R. Effect of solvent exposure on the filtration performance of electrostatically charged polypropylene filter media. Text. Res. J. 2009, 79 (4), 343-350.
- (20) Choi, H.-J.; Park, E.-S.; Kim, J.-U.; Kim, S. H.; Lee, M.-H. Experimental study on charge decay of electret filter due to organic solvent exposure. Aerosol Sci. Technol. 2015, 49 (10), 977-983.
- (21) Xiao, H.; Song, Y.; Chen, G. Correlation between charge decay and solvent effect for melt-blown polypropylene electret filter fabrics. J. Electrost. 2014, 72 (4), 311-314.
- (22) Chen, L.; Tian, G. L.; Wang, Y. F.; Ge, G. L. Method for onestep controllable synthesis of unimodal poly-dispersive nano and submicron silica particles, Patent, No. CN:201610807762:A.
- (23) Martin, S. B., Jr; Moyer, E. S. Electrostatic respirator filter media: filter efficiency and most penetrating particle size effects. Appl. Occup. Environ. Hyg. 2000, 15 (8), 609-617.
- (24) Qian, Y.; Orszag, S. Lattice BGK models for the Navier-Stokes equation: Nonlinear deviation in compressible regimes. Europhys. Lett. 1993, 21 (3), 255.
- (25) Qian, Y.; d'Humières, D.; Lallemand, P. Lattice BGK models for Navier-Stokes equation. Europhys. Lett. 1992, 17 (6), 479.
- (26) Hinds, W. C. Aerosol technology: properties, behavior, and measurement of airborne particles; John Wiley & Sons: New York,
- (27) Ounis, H.; Ahmadi, G. A comparison of Brownian and turbulent diffusion. Aerosol Sci. Technol. 1990, 13 (1), 47-53.
- (28) Wang, X. L.; Gidwani, A.; Girshick, S. L.; McMurry, P. H. Aerodynamic focusing of nanoparticles: II. Numerical simulation of particle motion through aerodynamic lenses. Aerosol Sci. Technol. **2005**, 39 (7), 624–636.
- (29) Ounis, H.; Ahmadi, G.; McLaughlin, J. B. Dispersion and deposition of Brownian particles from point sources in a simulated turbulent channel flow. J. Colloid Interface Sci. 1991, 147 (1), 233-
- (30) Hunter, R. J. Foundations of colloid science; Oxford University Press Inc.: New York, 2001.
- (31) Israelachvili, J. N. Intermolecular and surface forces; Elsevier (Singapore) Pte Ltd.: China, 2012; DOI: 10.1016/C2011-0-05119-0.
- (32) Wypych, G. Handbook of polymers, 2nd ed.; Chem Tec Publishing: Toronto, 2016; DOI: 10.1016/C2015-0-01462-9.
- (33) Pakarinen, O.; Foster, A.; Paajanen, M.; Kalinainen, T.; Katainen, J.; Makkonen, I.; Lahtinen, J.; Nieminen, R. Towards an accurate description of the capillary force in nanoparticle-surface interactions. Modell. Simul. Mater. Sci. Eng. 2005, 13 (7), 1175.

- (34) Greenler, R. G. Infrared study of the adsorption of methanol and ethanol on aluminum oxide. *J. Chem. Phys.* **1962**, *37* (9), 2094–2100
- (35) Wu, X.; Sacher, E.; Meunier, M. The effects of hydrogen bonds on the adhesion of inorganic oxide particles on hydrophilic silicon surfaces. *J. Appl. Phys.* **1999**, *86* (3), 1744–1748.
- (36) Guo, Z.; Zhao, T. Lattice Boltzmann model for incompressible flows through porous media. *Phys. Rev. E: Stat. Phys., Plasmas, Fluids, Relat. Interdiscip. Top.* **2002**, *66* (3), 036304.
- (37) Sbragaglia, M.; Succi, S. Analytical calculation of slip flow in lattice Boltzmann models with kinetic boundary conditions. *Phys. Fluids* **2005**, *17* (9), 093602.
- (38) Vazquez, G.; Alvarez, E.; Navaza, J. M. Surface tension of alcohol + water from 20 to 50 °C. *J. Chem. Eng. Data* **1995**, 40 (3), 611–614.
- (39) Brown, R. C. Air filtration: an integrated approach to the theory and applications of fibrous filters. Pergamon Press, Oxford, 1993.
- (40) Mizukami, M.; Moteki, M.; Kurihara, K. Hydrogen-bonded macrocluster formation of ethanol on silica surfaces in cyclohexane1. *J. Am. Chem. Soc.* **2002**, *124* (43), 12889–12897.
- (41) Mizukami, M.; Nakagawa, Y.; Kurihara, K. Surface induced hydrogen-bonded macrocluster formation of methanol on silica surfaces. *Langmuir* **2005**, *21* (21), 9402–9405.
- (42) Dupré, A. Théorie mécanique de la chaleur; Gauthier-Villars: Paris, 1869; pp 393-395.
- (43) Zhou, C. X.; Yuan, X. G.; Fan, L. T.; Zeng, A. W.; Yu, K. T.; Kalbassi, M.; Porter, K. E. Experimental study on contact angle of ethanol and N-propanol aqueous solutions on metal surfaces. *Distillation Absorption* **2010**, 359–364.
- (44) Buha, J.; Fissan, H.; Wang, J. Filtration behavior of silver nanoparticle agglomerates and effects of the agglomerate model in data analysis. *J. Nanopart. Res.* **2013**, *15* (7), 1709.
- (45) Gallyamov, M. O.; Tartsch, B.; Mela, P.; Börner, H.; Matyjaszewski, K.; Sheiko, S.; Khokhlov, A.; Möller, M. A scanning force microscopy study on the motion of single brush-like macromolecules on a silicon substrate induced by coadsorption of small molecules. *Phys. Chem. Chem. Phys.* **2007**, 9 (3), 346–352.
- (46) Kim, K. H.; Kim, J. B.; Ji, J. H.; Lee, S. B.; Bae, G. N. Nanoparticle formation in a chemical storage room as a new incidental nanoaerosol source at a nanomaterial workplace. *J. Hazard. Mater.* **2015**, 298, 36–45.
- (47) Jaworek, A.; Balachandran, W.; Krupa, A.; Kulon, J.; Lackowski, M. Wet electroscrubbers for state of the art gas cleaning. *Environ. Sci. Technol.* **2006**, 40 (20), 6197–6207.